REPORT DOCUMENTATION PAGE

Form Approved OMB NO. 0704-0188

1. REPORT DATE (DD-MM-YYYY)	2. REPORT TYPE	3. DATES COVERED (From - To)
27-08-2008	Final Report	13-Aug-2007 - 12-May-2008

4. TITLE AND SUBTITLE
Influence of Transport Processes on Autoignition of High Molecular Weight Fuels in Nonpremixed Flows

5a. CONTRACT NUMBER
W911NF-07-1-0521

5b. GRANT NUMBER

5c. PROGRAM ELEMENT NUMBER
611102

6. AUTHORS
Kalyanasundaram Seshadri

5d. PROJECT NUMBER

5e. TASK NUMBER

5f. WORK UNIT NUMBER

7. PERFORMING ORGANIZATION NAMES AND ADDRESSES
University of California - San Diego
Office of Contract & Grant Administration
9500 Gilman Drive
La Jolla, CA 92093 -0934

8. PERFORMING ORGANIZATION REPORT NUMBER

9. SPONSORING/MONITORING AGENCY NAME(S) AND ADDRESS(ES)
U.S. Army Research Office
P.O. Box 12211
Research Triangle Park, NC 27709-2211

10. SPONSOR/MONITOR'S ACRONYM(S)
ARO

11. SPONSOR/MONITOR'S REPORT NUMBER(S)
53430-EG-II.1

12. DISTRIBUTION AVAILIBILITY STATEMENT
Approved for Public Release; Distribution Unlimited

13. SUPPLEMENTARY NOTES
The views, opinions and/or findings contained in this report are those of the author(s) and should not contrued as an official Department of the Army position, policy or decision, unless so designated by other documentation.

14. ABSTRACT
The objective of this research is to obtain an improved understanding of the influences of transport processes, chemical kinetics and flow characteristics on the mechanisms of autoignition of condensed (liquid) hydrocarbon fuels in nonpremixed, nonuniform flows. An experimental and numerical investigation is carried out. The condensed fuels tested are n-heptane and n-decane. Recent experimental investigation of autoignition of liquid hydrocarbon fuels, in particular n-heptane and n-decane, show that at low strain rate it is easier to ignite n-decane, while at high values of the strain rate it is easier to ignite n-heptane. Experiments were conducted employing the ``counterflow configuration''. Critical conditions of autoignition were measured.

15. SUBJECT TERMS
Surrogate fuels, JP-8, autoignition, nonpremixed flames

16. SECURITY CLASSIFICATION OF:			17. LIMITATION OF ABSTRACT	15. NUMBER OF PAGES	19a. NAME OF RESPONSIBLE PERSON
a. REPORT	b. ABSTRACT	c. THIS PAGE			Kalyanasundaram Seshadri
U	U	U	SAR		19b. TELEPHONE NUMBER 858-534-4876

Standard Form 298 (Rev 8/98)
Prescribed by ANSI Std. Z39.18

Report Title

Influence of Transport Processes on Autoignition of High Molecular Weight Fuels in Nonpremixed Flows

ABSTRACT

The objective of this research is to obtain an improved understanding of the influences of transport processes, chemical kinetics and flow characteristics on the mechanisms of autoignition of condensed (liquid) hydrocarbon fuels in nonpremixed, nonuniform flows. An experimental and numerical investigation is carried out. The condensed fuels tested are n-heptane and n-decane. Recent experimental investigation of autoignition of liquid hydrocarbon fuels, in particular n-heptane and n-decane, show that at low strain rate it is easier to ignite n-decane, while at high values of the strain rate it is easier to ignite n-heptane. Experiments were conducted employing the ``counterflow configuration". Critical conditions of autoignition were measured. The mass fractions of fuel close to the liquid gas interface were measured. With increasing strain rate the mass fraction of n-heptane at the liquid-gas interface increases more rapidly than that of n-decane. This the reason why n-heptane is easier to ignite when compared to n-decane at high values of the strain rate.

List of papers submitted or published that acknowledge ARO support during this reporting period. List the papers, including journal references, in the following categories:

(a) Papers published in peer-reviewed journals (N/A for none)

Number of Papers published in peer-reviewed journals: 0.00

(b) Papers published in non-peer-reviewed journals or in conference proceedings (N/A for none)

Number of Papers published in non peer-reviewed journals: 0.00

(c) Presentations

Number of Presentations: 0.00

Non Peer-Reviewed Conference Proceeding publications (other than abstracts):

Number of Non Peer-Reviewed Conference Proceeding publications (other than abstracts): 0

Peer-Reviewed Conference Proceeding publications (other than abstracts):

Number of Peer-Reviewed Conference Proceeding publications (other than abstracts): 0

(d) Manuscripts

Number of Manuscripts: 0.00

Number of Inventions:

Graduate Students

NAME	PERCENT_SUPPORTED
Ulrich Niemann	0.25
Patrick Weydert	0.49
Niek Tiemessen	0.49
FTE Equivalent:	**1.23**
Total Number:	**3**

Names of Post Doctorates

NAME	PERCENT_SUPPORTED
FTE Equivalent:	
Total Number:	

Names of Faculty Supported

NAME	PERCENT_SUPPORTED	National Academy Member
Kalyanasundaram Seshadri		No
FTE Equivalent:		
Total Number:	**1**	

Names of Under Graduate students supported

NAME	PERCENT_SUPPORTED
FTE Equivalent:	
Total Number:	

Student Metrics

This section only applies to graduating undergraduates supported by this agreement in this reporting period

The number of undergraduates funded by this agreement who graduated during this period:	0.00
The number of undergraduates funded by this agreement who graduated during this period with a degree in science, mathematics, engineering, or technology fields:.....	0.00
The number of undergraduates funded by your agreement who graduated during this period and will continue to pursue a graduate or Ph.D. degree in science, mathematics, engineering, or technology fields:.....	0.00
Number of graduating undergraduates who achieved a 3.5 GPA to 4.0 (4.0 max scale):	0.00
Number of graduating undergraduates funded by a DoD funded Center of Excellence grant for Education, Research and Engineering:	0.00
The number of undergraduates funded by your agreement who graduated during this period and intend to work for the Department of Defense	0.00
The number of undergraduates funded by your agreement who graduated during this period and will receive scholarships or fellowships for further studies in science, mathematics, engineering or technology fields:	0.00

Names of Personnel receiving masters degrees

NAME
Patrick Weydert
Total Number: 1

Names of personnel receiving PHDs

NAME
Total Number:

Names of other research staff

NAME	PERCENT_SUPPORTED
FTE Equivalent:	
Total Number:	

Sub Contractors (DD882)

Inventions (DD882)

Influence of Transport Processes on Autoignition of High Molecular Weight Hydrocarbon Fuels in Nonpremixed Flows, Agreement Number: W911NF0710521

Contents

1 Statement of Problem Studied

The Department of Defense directive # 4140.25 dated April 12, 2004 mandates that "primary fuel support for land-based air and ground forces in all theaters (overseas and in the Continental United States) shall be accomplished using a single kerosene-based fuel, in order of precedence: JP-8, commercial jet fuel (with additive package), or commercial jet fuel (without additives)." A key challenge is to develop technologies for converting diesel-powered equipment employed by the US Army so that they can be powered by JP-8. This conversion is a complicated process. Many issues with fuel properties and performance have to be considered. They include autoignition, combustion, fuel injection, lubricity, and spray characteristics.

The objective of the study described in this report is to obtain an improved understanding of the fundamental mechanisms of autoignition of condensed (liquid) hydrocarbon fuels in nonpremixed, nonuniform flows. The fuels considered are components of surrogates of gasoline, diesel and JP-8. Experimental and numerical studies are carried out. JP-8 is a mixture of numerous aliphatic and aromatic compounds. The major components of this fuel are straight chain paraffins, branched chain paraffins, cycloparaffins, aromatics, and alkenes [1, 2]. Recently the U. S. Army Research Office (ARO) and the Air Force Office of Scientific Research (AFOSR) have sponsored several workshops on surrogate fuels for gasoline, diesel and jet fuels. In these workshops strategies for developing surrogates were discussed. Also suggestions were made concerning the choice of components for the surrogates.

Recent experimental investigation of autoignition of liquid hydrocarbon fuels, in particular *n*-heptane and *n*-decane, show that at low strain rates it is easier to ignite *n*-decane, while at strain rates it is easier to ignite *n*-heptane [3]. The reason for this change in relative order of ignition was not understood. It has been suggested at the ARO/AFOSR workshop on surrogate fuels that this is an important problem that must be understood because it impacts on the development of surrogate fuels. The research described in this report addressed this question.

2 Previous Research

The Propulsion and Energetics division of the U. S. Army Research Office supported at the University of California at San Diego a research project entitled "Autoignition and Combustion of Diesel and JP-8,". The principal objective of this research was to develop surrogate fuels that can reproduce combustion characteristics of diesel, JP-8 and Fisher Tropsch (FT) JP-8. The combustion characteristics include 1) autoignition and extinction characteristics in nonpremixed systems, 2) ignition delay times in premixed systems, 3) temperature and concentrations histories in flow reactors, and 4) burning velocities in premixed systems. Ex-

perimental and numerical studies were carried out.

To capture the influence of the flow field on the critical conditions of autoignition, experiments were conducted in the counterflow configuration. Two types of configuration—the condensed fuel configuration and the prevaporized fuel configuration were employed in the experimental study. A schematic illustration of the condensed fuel configuration is shown in Fig. 1. An axisymmetric stagnation-point flow of a gaseous oxidizer stream over the surface of an evaporating pool of a liquid fuel is considered. The oxidizer stream is a mixture of oxygen

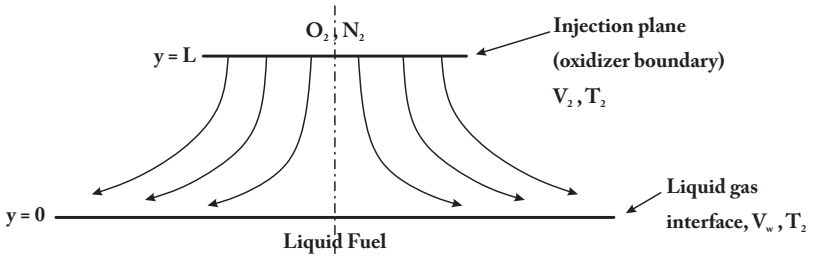

Figure 1: Schematic illustration of the condensed fuel configuration. V_2 and $V_{\rm w}$ are the velocities at the oxidizer boundary and on the gas side of the liquid-gas interface, respectively. T_2 and $T_{\rm w}$ are the temperatures at the oxidizer boundary and the liquid-gas interface, respectively.

(O_2) and nitrogen (N_2). It is injected from the oxidizer-duct. The exit of the oxidizer-duct is the oxidizer boundary. The distance between the surface of the liquid pool and the oxidizer boundary is L. At the oxidizer boundary, the magnitude of the injection velocity V_2, the temperature T_2, the density ρ_2, and the mass fraction of oxygen $Y_{\rm O_2,2}$. Here subscript 2 represents conditions at the oxidizer boundary. On the gas side of the liquid-gas interface, the temperature is $T_{\rm w}$, the mass fraction of fuel is $Y_{\rm F,w}$, and the mass averaged velocity is $V_{\rm w}$. Here subscript w represents conditions on the gas side of the liquid-gas interface. The studies were carried out for $T_{\rm w} < T_2$.

In the condensed fuel configuration, a stagnation plane is established between the oxidizer stream that is injected from the oxidizer boundary at a velocity V_2, and the blowing velocity at the surface of the liquid pool $V_{\rm w}$. The structure of the flow field depends on the Reynolds numbers, $Re_2 = \rho_2 V_2 L/\mu_2$, and $Re_{\rm w} = \rho_{\rm w} V_{\rm w} L/\mu_{\rm w}$. Here μ_2 and $\mu_{\rm w}$ are the coefficients of viscosity at the oxidizer boundary and on the gas side of the liquid-gas interface and $\rho_{\rm w}$ is the density on the gas side of the liquid-gas interface. The value of Re_2 is large and that of $Re_{\rm w}$ is small. If $Re_{\rm w} < Re_2^{1/2}$, a thin viscous boundary layer will develop close to the liquid-gas interface, the stagnation plane will be established inside this boundary layer [4]. The flow outside this viscous boundary layer will be nonreactive, inviscid and rotational. Chemical reactions take place in the viscous boundary layer. The thickness of this boundary layer will

decrease with increasing Re_2. It has been shown that the strain rate at the stagnation plane, a_2, is given by [4]

$$a_2 = 2V_2/L. \tag{1}$$

The values of $T_{\rm w}$ and $Y_{\rm F,w}$ depend on the kinetics of vaporization. In general the value of $T_{\rm w}$ will be lower than the normal boiling point, $T_{\rm b}$. The spatial gradient of temperature and the spatial gradient of mass fraction of the fuel at the liquid-gas interface will not be zero. The heat flux at the surface of the liquid fuel will be balanced by the product of the burning rate and heat of vaporization. The flux of fuel evaporating from the surface of the liquid fuel will be balanced by the burning rate. The flux of all other species will be zero at the surface of the liquid fuel.

Critical conditions of autoignition were measured for hydrocarbon fuels employing the condensed fuel configuration. The fuels tested were, *n*-heptane (C_7H_{16}), *n*-octane (C_8H_{18}), *n*-decane ($C_{10}H_{22}$), *n*-dodecane ($C_{12}H_{26}$), *n*-hexadecane ($C_{16}H_{34}$), *iso*-octane (C_8H_{18}), JP-8, and diesel. The oxidizer stream was air. At a given value of V_2 and $T_2 < T_{2,\rm I}$ the flow field was established. Here $T_{2,\rm I}$ is the temperature of the oxidizer stream at which autoignition takes place. The temperature of the oxidizer stream was gradually increased until autoignition takes place. The values $T_{2,\rm I}$ and V_2 were recorded. The strain rate at autoignition, $a_{2,\rm I}$, was calculated using Eqn. (1). Figure 2 shows $T_{2,\rm I}$ as a function of $a_{2,\rm I}$. Here the symbols represent

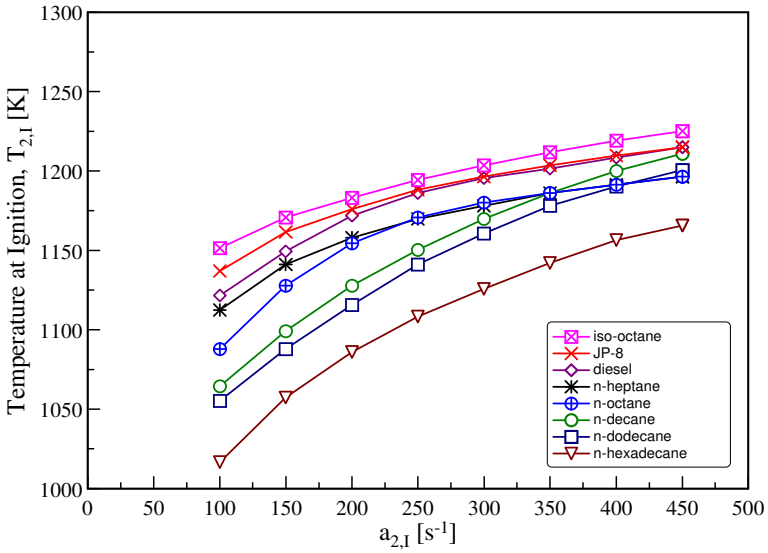

Figure 2: The temperature of air, $T_{2,\rm I}$, as a function of the strain rate, $a_{2,\rm I}$ at autoignition for straight-chain alkanes, *iso*-octane, JP-8, and diesel. The symbols represent measurements. The lines are best fits to the experimental data. The experimental data was obtained employing the condensed fuel configuration shown in Fig. 1.

measurements and the lines are best fits to the experimental data. At a given value of strain rate, autoignition will take place if the temperature of the oxidizer stream is greater than $T_{2,\mathrm{I}}$. Experimental data, for a given fuel, shows that the value of $T_{2,\mathrm{I}}$ increases with increasing $a_{2,\mathrm{I}}$. Figure 2 shows that at low values of $a_{2,\mathrm{I}}$, *iso*-octane is the most difficult to ignite followed by JP-8, diesel, *n*-heptane, *n*-octane, *n*-decane, *n*-dodecane , and *n*-hexadecane. At high values of the strain rate the order is changed. Figure 2 shows that at high values of the strain rate, *iso*-octane is the most difficult to ignite followed by JP-8 and diesel, *n*-decane, *n*-dodecane, *n*-heptane and *n*-octane, and *n*-hexadecane. This change in order has an impact on the selection of surrogate fuels, because at low strain rate the critical conditions of autoignition of *n*-heptane is close to that for JP-8, while at high values of the strain rate the critical conditions of autoignition of *n*-decane is close to that for JP-8. The research described here investigated the reason for the change in order of reactivity for *n*-heptane and *n*-decane.

3 Summary of the Most Important Results

Experimental and numerical studies were carried out to investigate the influence of transport processes on critical conditions of autoignition of high molecular weight hydrocarbon fuels. The fuels considered were *n*-heptane and *n*-decane. The studies were carried out at a pressure of one atmosphere. The condensed fuel configuration shown in Fig. 1 and the prevaporized fuel configuration shown in Fig. 3 were employed in the study. In the condensed fuel configuration the vaporization and transport processes at the liquid-gas interface are similar to those taking place at the surface of liquid droplets that are injected into the combustion chamber of practical systems. A key limitation of this configuration is that the temperature, T_{w}, and the mass fraction of the fuel, $Y_{\mathrm{F,w}}$ at the liquid-gas interface depend on the kinetics of vaporization and cannot be independently changed. This limitation is overcome in the prevaporized fuel configuration. Here a fuel stream made up of prevaporized fuel and nitrogen is injected from one duct and an oxidizer stream made up of oxygen and nitrogen is injected from the other duct. The velocities of the fuel stream and the oxidizer stream at the injection planes are represented by V_1 and V_2, respectively. The temperatures of the fuel stream and the oxidizer stream at the injection planes are represented by T_1 and T_2, respectively. The distance between the injection planes is L. The strain rate on the oxidizer side of the stagnation plane is given by the expression [4]

$$a = \frac{2|V_2|}{L}\left(1 + \frac{|V_1|\sqrt{\rho_1}}{|V_2|\sqrt{\rho_2}}\right), \tag{2}$$

where ρ_2 and ρ_1 are, respectively, the density of the oxidizer stream and the fuel stream at the injection planes. In the prevaporized fuel configuration it is possible to independently control the values of temperature, T_1, and mass fraction of fuel, $Y_{\mathrm{F},1}$ at the fuel boundary. This will allow us, for example, to carry out experiments with *n*-heptane and *n*-decane at the same

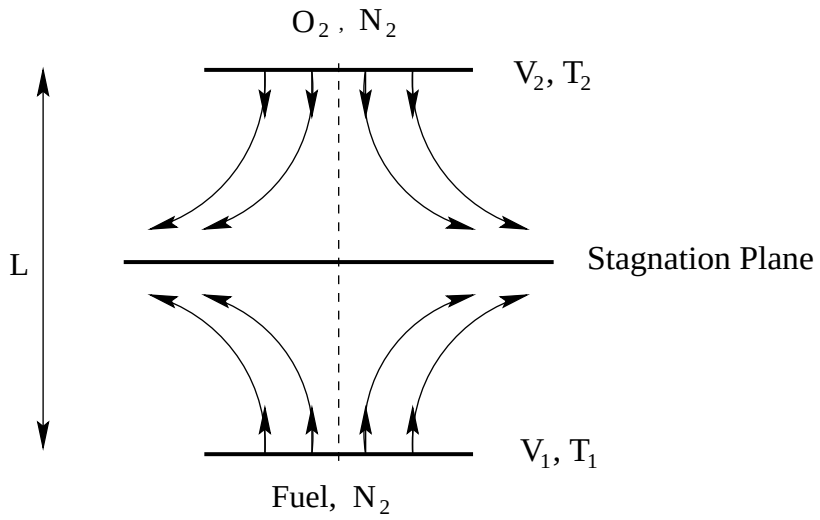

Figure 3: Schematic illustration of the prevaporized fuel configuration. V_2 and T_2 are the velocity and temperature at the oxidizer-injection plane and V_1 and T_1 are the velocity and temperature at the fuel-injection plane.

values of T_1, and $Y_{\mathrm{F},1}$ although their kinetics of vaporization are different.

3.1 Experimental Studies Employing the Prevaporized Fuel Configuration

The parameters that influence autoignition in the prevaporized fuel configuration are (1) composition of the fuel stream, $Y_{\mathrm{F},1}$, (2) temperature of the fuel stream, T_1, (3) composition of the oxidizer stream, $Y_{\mathrm{O}_2,2}$, (4) temperature of the oxidizer stream, T_2, (5) strain rate, a_2, and (6) pressure, p. Experiments were carried out at fixed values of $T_1 = 473\,\mathrm{K}$, $Y_{\mathrm{F},1} = 0.4$, and $Y_{\mathrm{O}_2,2} = 0.233$ (air). At a given value of V_2 and $T_2 < T_{2,\mathrm{I}}$ the flow field is established. The temperature of the oxidizer stream is gradually increased until autoignition takes place. The values $T_{2,\mathrm{I}}$ and V_2 are recorded. The strain rate at autoignition, $a_{2,\mathrm{I}}$, is calculated using Eqn. (1). Figure 4 shows the temperature of air, $T_{2,\mathrm{I}}$, as a function of the strain rate, $a_{2,\mathrm{I}}$ at autoignition for *n*-heptane and *n*-decane. At a given value of strain rate the value of $T_{2,\mathrm{I}}$ for *n*-heptane is higher than that for *n*-decane. Thus *n*-heptane is more difficult to ignite in comparison to *n*-decane for all values of the strain rate. The agrees with the order shown in Figure 2 at low value of the strain rates but not with the order shown at the high values of the strain rates. This is examined further.

3.2 Experimental Studies Employing the Condensed Fuel Configuration

Figure 5 shows a schematic illustration of the experimental apparatus employing the condensed fuel configuration shown in Fig. 1. The apparatus comprises the liquid-fuel burner and

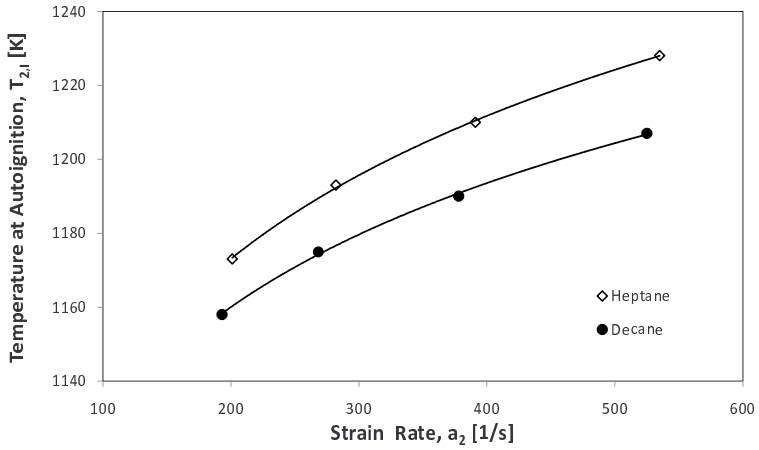

Figure 4: The temperature of air, $T_{2,\mathrm{I}}$, as a function of the strain rate, $a_{2,\mathrm{I}}$ at autoignition for $T_1 = 473\,\mathrm{K}$, $Y_{\mathrm{F},1} = 0.4$, and $Y_{\mathrm{O}_2,2} = 0.233$ (air). The symbols represent measurements. The lines are best fits to the experimental data. The experimental data was obtained employing the prevaporized fuel configuration shown in Fig. 3.

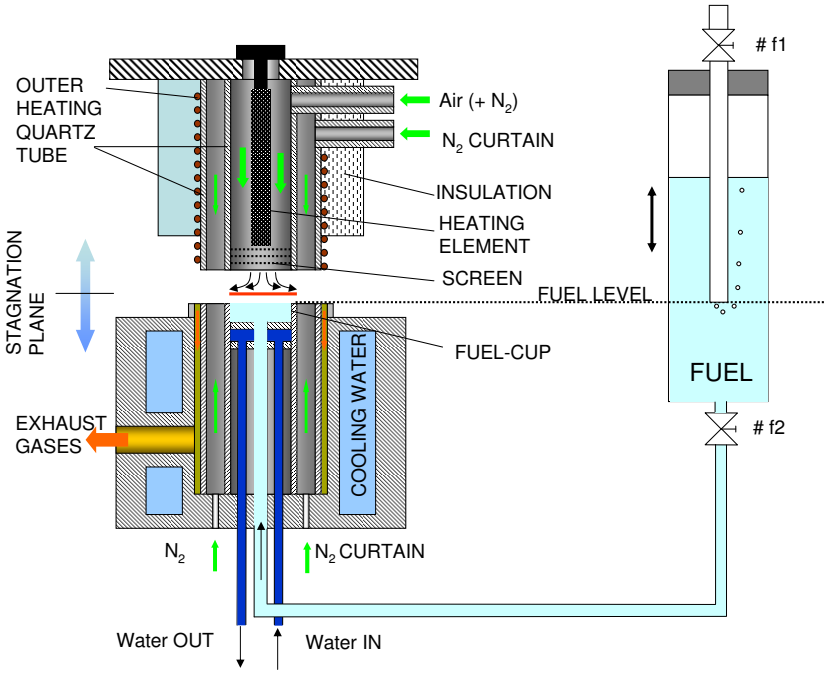

Figure 5: Schematic illustration of the experimental setup.

the fuel reservoir. The liquid-fuel burner is made up of two parts: the bottom part comprises the fuel-cup, the exhaust system, and the cooling system, while the top part comprises the oxidizer-duct and heating elements. Liquid fuel flows from the reservoir to the fuel-cup. The reservoir accurately maintains, at a constant value, the amount of fuel in the cup, by matching the mass rate of fuel flowing from the reservoir to the fuel-cup to the burning rate. Further details concerning the reservoir are described elsewhere [5, 6].

The fuel-cup has an inner diameter of 35 mm and the depth is 10 mm. From an annular region that surrounds the fuel duct, a "curtain" flow of nitrogen flows upward. A cooling system surrounds this "curtain" nitrogen flow. Hot gases that are formed in the mixing-layer between the surface of the liquid pool and the oxidizer boundary enter this cooling system. Here the hot gases are cooled by water, that is sprayed from a nozzle, before they enter the exhaust system. The oxidizer-duct is made of quartz. The inner diameter of the oxidizer-duct is 23.5 mm. Near the exit of the oxidizer-duct several nichrome wire screens (100 mesh) are placed to make the velocity profile uniform. From an annular region that surrounds the oxidizer-duct a "curtain" flow of nitrogen flows parallel to the oxidizer stream. The air flowing inside the oxidizer-duct is heated by a silicon carbide heating element placed inside the oxidizer-duct. Additional heating is provided by wires wrapped around the quartz duct. To minimize heat losses, a blanket is wrapped around the the top part of the burner. The distance between the surface of the liquid pool and the oxidizer boundary is $L = 12\,\text{mm}$.

All gaseous flowrates are measured by computer-regulated mass flow controllers. The calibrated accuracy of these mass flow controllers is $\pm 1\%$. The temperature of the air at the exit of the oxidizer boundary, T_2, is measured using a Pt-Pt 13% Rh thermocouple with wire diameter of 0.07 mm and a junction diameter of 0.21 mm. The measured temperature is corrected for radiative heat losses assuming spherical shape of the junction, a constant Nusselt number of 2.0, and a constant emissivity of 0.2 [7]. The accuracy of the corrected temperature is expected to be better than ± 25 K. The velocity of air at the oxidizer boundary, V_2, is presumed to be equal to the ratio of the volumetric flow-rate of air to the cross-section area of the oxidizer-duct.

The parameters that influence autoignition in the condensed fuel configuration are: (1) composition of the oxidizer stream, $Y_{O_2,2}$, (2) temperature of the oxidizer stream, T_2, (3) strain rate a_2, and (4) pressure, p. The experiments were conducted with $Y_{O_2,2} = 0.233$ (air). At a given value of V_2 and $T_2 < T_{2,I}$ the flow field was established. The temperature of the oxidizer stream was gradually increased until autoignition takes place. The values $T_{2,I}$ and V_2 were recorded. The strain rate at autoignition, $a_{2,I}$, was calculated using Eqn. (1). Figure 6 shows the critical conditions of autoignition for *n*-heptane and *n*-decane. The experimental

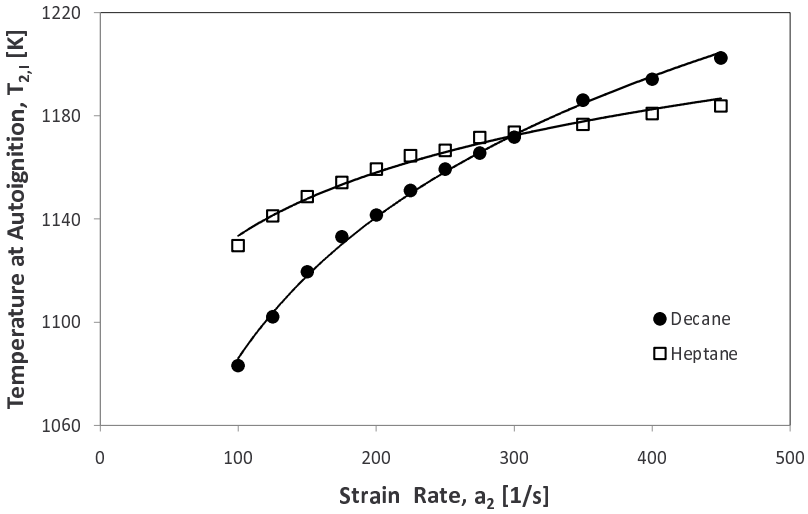

Figure 6: The temperature of air, $T_{2,\mathrm{I}}$, as a function of the strain rate, $a_{2,\mathrm{I}}$ at autoignition for $Y_{\mathrm{O}_2,2} = 0.233$ (air). The symbols represent measurements. The lines are best fits to the experimental data. The experimental data was obtained employing the condensed fuel configuration shown in Fig. 1.

data in Fig. 6 agree with that shown in Fig. 2 for *n*-heptane and *n*-decane. At low values of the strain rate, *n*-decane is easier to ignite when compared with *n*-heptane while at high values of the strain rate *n*-heptane is easier to ignite.

3.3 Numerical Calculations

To investigate the fundamental reasons for the qualitative differences between the ignition characteristics of *n*-heptane and *n*-decane illustrated in Figs. 4 and 6, numerical calculations were performed using detailed chemical-kinetic mechanism for *n*-heptane and *n*-decane. For *n*-heptane the mechanism described in Refs. [8, 9] were employed while for *n*-decane the mechanism described in Ref. [10] was used. Calculations were performed using the condensed fuel configuration shown in Fig. 1. Boundary conditions are applied at the exit of the oxidizer-duct and at the liquid-gas interface. At the exit of the oxidizer-duct, the temperature, T_2, the composition, $Y_{\mathrm{O}_2,2}$, and the injection velocity, V_2, of the oxidizer stream is specified. The tangential component of the flow velocity at the injection plane is zero. At the liquid gas interface, the no slip boundary condition is applied. The temperature is assumed to be the boiling point of the liquid fuel. The flux of all species except that of the fuel is zero. The heat flux into the liquid pool is balanced by the product of the burning rate and the heat of vaporization.

Figures 7 and 8 show that at a given value of the strain rate, the calculated values of

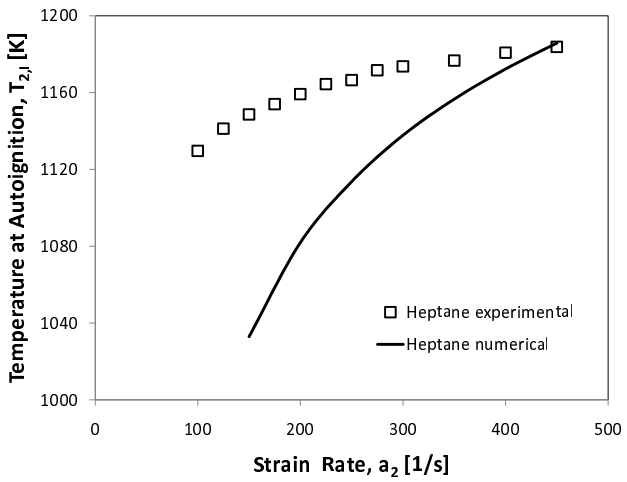

Figure 7: The temperature of air, $T_{2,\mathrm{I}}$, as a function of the strain rate, $a_{2,\mathrm{I}}$ at autoignition for $Y_{\mathrm{O}_2,2} = 0.233$ (air). The fuel is *n*-heptane. The symbols represent measurements. The lines are results of numerical calculations. The experimental data and calculations employed the condensed fuel configuration shown in Fig. 1.

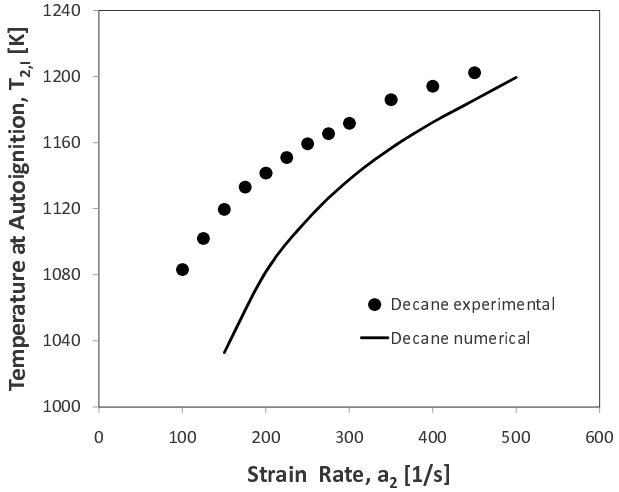

Figure 8: The temperature of air, $T_{2,\mathrm{I}}$, as a function of the strain rate, $a_{2,\mathrm{I}}$ at autoignition for $Y_{\mathrm{O}_2,2} = 0.233$ (air). The fuel is *n*-decane. The symbols represent measurements. The lines are results of numerical calculations. The experimental data and calculations employed the condensed fuel configuration shown in Fig. 1.

the $T_{2,\mathrm{I}}$ is greater than the measured values. The calculated values of critical conditions of autoignition do not agree with the experimental data, therefore they do not provide the reasons for the qualitative differences between the autoignition characteristics of *n*-heptane and *n*-decane.

3.3.1 Influence of Diffusion Coefficients

Figure 9 compares the critical conditions of autoignition calculated using the detailed mechanism with those calculated with the diffusion coefficient of *n*-heptane changed to that of *n*-decane. There is very little difference between the calculated values. Figure 10 shows simi-

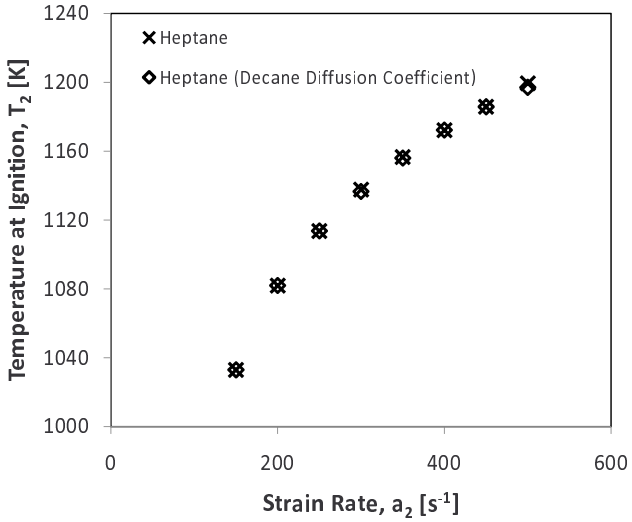

Figure 9: The calculated values of the temperature of air, $T_{2,\mathrm{I}}$, as a function of the strain rate, $a_{2,\mathrm{I}}$ at autoignition for $Y_{\mathrm{O}_2,2} = 0.233$ (air). The fuel is *n*-heptane. The calculations employed the condensed fuel configuration shown in Fig. 1. The figure illustrates the influence of diffusion coefficients on critical conditions of autoignition.

lar comparison for *n*-decane. Thus the qualitative differences between the critical conditions of autoignition between *n*-heptane and *n*-decane shown in Fig. 6 cannot be attributed to differences in diffusivities between *n*-heptane and *n*-decane.

3.3.2 Influence of flow field

To characterize the influence of the flow field the concentration of the fuel was measured 1 mm above the liquid-gas interface. The measurements were made for various values of the strain rate and at a value of T_2 that is less than the autoignition temperature by 5 K. Figure 11 shows the measured mass fraction of *n*-heptane and *n*-decane as a function of the strain rate. The mass fractions increase with increasing strain rate. At a given value of the strain rate

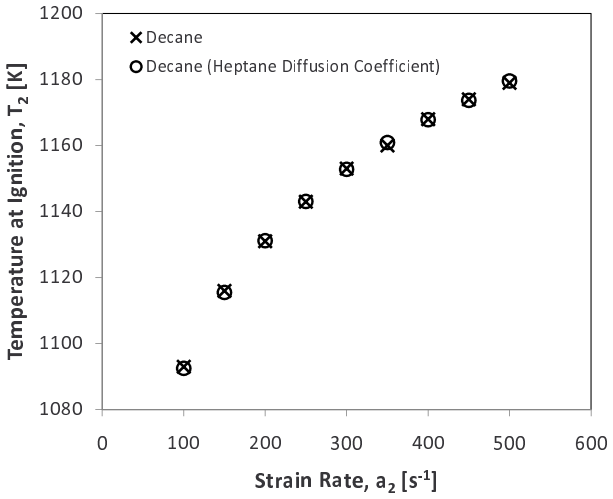

Figure 10: The calculated values of the temperature of air, $T_{2,\mathrm{I}}$, as a function of the strain rate, $a_{2,\mathrm{I}}$ at autoignition for $Y_{\mathrm{O}_2,2} = 0.233$ (air). The fuel is n-decane. The calculations employed the condensed fuel configuration shown in Fig. 1. The figure illustrates the influence of diffusion coefficients on critical conditions of autoignition.

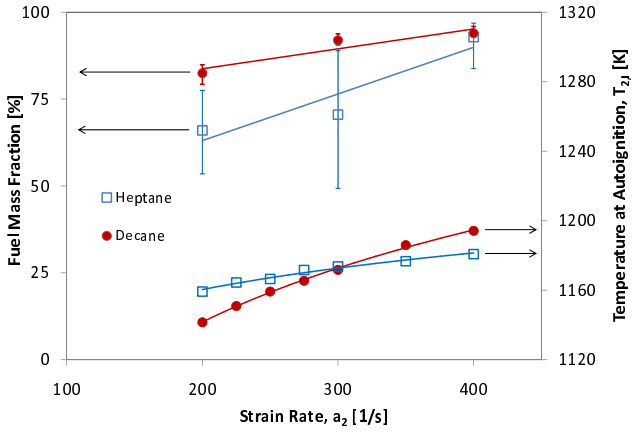

Figure 11: The mass fraction of the fuel at 1 mm above the liquid-gas interface as a function of strain rate. The measurements were made at a value of T_2 that is less than the autoignition temperature by 5 K. The value of temperature of the oxidizer stream at autoignition is also shown.

the value of $T_{2,\mathrm{I}}$ increases with increasing value of $Y_{\mathrm{F},1}$. Figure 11 shows that the increase in the mass fraction of *n*-heptane is steeper than that of *n*-decane. Thus, the relatively higher mass fraction of *n*-heptane in comparison to that of *n*-decane at higher values of the strain rate appears to be the reason why heptane is easier to ignite at high values of the strain rate.

3.4 Summary and Conclusions

The present research was carried out to investigate the reason why *n*-decane is easier to ignite in comparison to *n*-heptane at low strain rates while *n*-heptane is easier to ignite at high strain rates. Experiments were carried out employing the condensed fuel configuration shown in Fig. 1 and the prevaporized fuel configuration shown in Fig. 3. The results obtained in the prevaporized fuel configuration (Fig. 4) show that *n*-decane is easier to ignite when compared with *n*-heptane for all values of the strain rate. This is different from the data obtained using the condensed fuel configuration (Fig. 6). Thus the qualitative differences between the results obtained in these configurations cannot be attributed to the diffusion coefficients of *n*-heptane and *n*-decane. This is confirmed by the calculated values of critical conditions of autoignition. Figure 9 shows that the critical conditions of autoignition of *n*-heptane does not change if the diffusion coefficient of *n*-heptane is changed to that of *n*-decane. Similar results are obtained for *n*-decane as shown in Fig. 10. The concentration of fuel was measured at a distance of 1 mm above the liquid-gas interface. The results show (Fig. 11) that the concentration of *n*-heptane increases more rapidly than that of *n*-decane. This is the reason why it is easier to ignite *n*-heptane at high values of the strain rate. Future work should focus on improving the chemical-kinetic mechanism of *n*-heptane and *n*-decane, so the the critical conditions of autoignition calculated using these mechanisms agree better with experimental data.

References

[1] T. Edwards and L. Q. Maurice. Surrogate mixtures to represent complex aviation and rocket fuels. *Journal of Propulsion and Power*, 17:461–466, 2001.

[2] T. Edwards. "Real" kerosene aviation and rocket fuels: Compositions and surrogates. *2001 Fall Technical Meeting, Eastern States Section of the Combustion Institute*, 2001.

[3] S. Humer, R. Seiser, and K. Seshadri. Autoignition and extinction of hydrocarbon fuels in nonpremixed systems. In *3*$^{\mathrm{rd}}$ *Joint Meeting of the United States Sections of the Combustion Institute*, Paper B26, The University of Illinois at Chicago, 2003.

[4] K. Seshadri and F. A. Williams. Laminar flow between parallel plates with injection of a reactant at high Reynolds number. *International Journal of Heat and Mass Transfer*, 21(2):251–253, 1978.

[5] S. N. Bajpai. Extinction of vapor fed diffusion flames by halons 1301 and 1211-Part I. Technical Report 22430, Factory Mutual Research Corporation, Norwood, Massachusetts, 1974.

[6] K. Seshadri. *Studies on Flame Extinction.* Ph.D thesis, University of California at San Diego, Department of Applied Mechanics and Engineering Sciences, 1977.

[7] T. Weißweiler. Measurements of stable species and soot volume fraction in a propane-air counterflow diffusion flame. Diploma thesis, Institut für Allgemeine Mechanik, RWTH Aachen, Aachen, Germany, 1994.

[8] R. Seiser. *Nonpremixed Combustion of Liquid Hydrocarbon Fuels.* Ph.D thesis, Technical University of Graz, 2000.

[9] R. Seiser, H. Pitsch, K. Seshadri, W. J. Pitz, and H. J. Curran. Extinction and autoignition of n-heptane in counterflow configuration. *Proceedings of the Combustion Institute*, 28:2029–2037, 2000.

[10] G. Bikas and N. Peters. Kinetic modelling of n-decane combustion and autoignition. *Combustion and Flame*, 126:1456–1475, 2001.